Conf-950793--19

LA-UR- 95-2459

Title: X-RAY EMISSION FROM COLLIDING LASER PLASMAS

Author(s): MARK D. WILKE
ANDREW W. OBST
D. WINSKE
MICHAEL E. JONES
STUART A. BAKER
JOSEPH ABDALLAH, JR.
STEPHEN E. CALDWELL
ROBERT G. WATT
S. ROBERT GOLDMAN
BRUNO S. BAUER
R. B. GIBSON

Submitted to: SPIE CONFERENCE

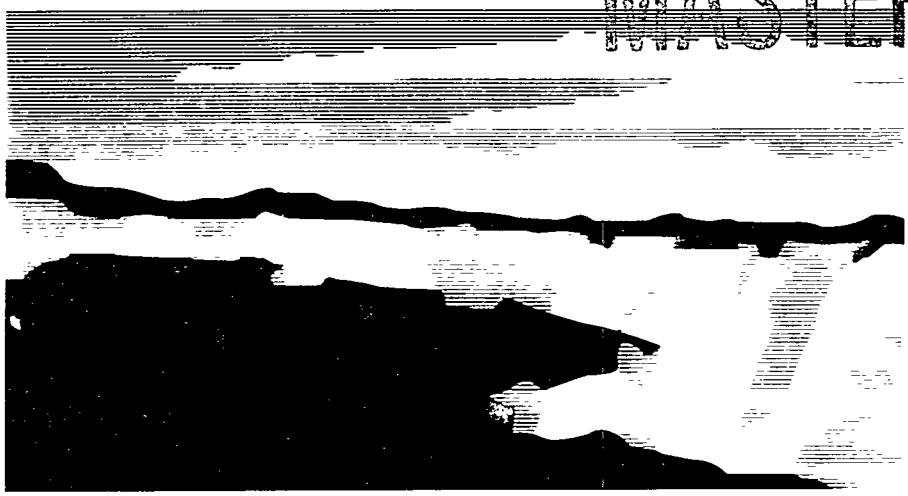

Los Alamos
NATIONAL LABORATORY

Form No. 836 R5
ST 2629 10/91

X-ray emission from colliding laser plasmas

Mark Wilke, Andrew W. Obst, D. Winske, Michael E. Jones, Stuart A. Baker[1], Joseph Abdallah, Jr., Stephen E. Caldwell, Robert G. Watt, S. Robert Goldman, Bruno S. Bauer[2] and R. B. Gibson.

Los Alamos National Laboratory
Los Alamos, New Mexico 87545

[1]EG&G/EM-Los Alamos Operations
Los Alamos, New Mexico 87545

[2]Lawrence Livermore National Laboratory
Livermore, California 94551

ABSTRACT

Colliding Au, CD and Ti-Cr plasmas have been generated by illuminating two opposing foils each with a ~100J, 0.5 nsec, 2ω Nd-glass laser beam from the Trident laser facility at Los Alamos. The plasmas are being used to study plasma interactions which span the parameter regime from interpenetrating to collisional stagnation. X-ray emission during the laser target interaction and the subsequent collision is used to diagnose the initial plasma conditions and the colliding plasma properties. X-ray instrumentation consists of a 100 ps gated x-ray pinhole imager, a time-integrated bremsstrahlung x-ray spectrograph and a gated x-ray spectrograph used to record isoelectronic spectra from the Ti-Cr plasmas. The imager has obtained multi-frame images of the collision and therefore, a measure of the stagnation length which is a function of the ion charge state and density and a strong function of the electron temperature. Other instrumentation includes a Thomson scattering spectrometer with probe beam, neutron detectors used to monitor the CD coated foil collisions and an ion spectrometer. We will describe the current status of the experiments and current results with emphasis on the x-ray emission diagnostics. We will also briefly describe the modeling using Lasnex and ISIS, a particle-in-cell code with massless fluid electrons and inter particle (classical) collisions.

Keywords: colliding plasmas, x-ray imaging, x-ray spectroscopy, inertial confinement fusion

INTRODUCTION

There are many examples of plasma studies where the plasma Coulomb mean free path is either large compared to the plasma dimensions of interest or much shorter than the plasma scale. In the former case, collisionless processes are important in generating spatial inhomogeneities such as collisionless shocks[1] of which the earth's bow wave is a well known example. In the later case gas dynamic processes such as classical shock waves are important[2]. A less studied regime is the transition or semi-collisional regime where the Coulomb mean free path is comparable to the plasma dimension of interest. There have been theoretical[3] and experimental[4-6] studies of low to middle-Z, planar collisions of laser generated plasmas relevant to x-ray laser experiments. Colliding Au plasmas in a cylindrical geometry as well as a planar geometry were indirectly investigated at low temperatures (30 to 45 eV) as part of a study of laser and radiation transport along cylindrical capillaries[7]. More recently, axial images of gold laser fusion target hohlraums indicate plasma processes leading to collision and stagnation of plasmas on the hohlraum axis[8].

Calculational tools have also become more sophisticated at handling semi-collisional plasmas. Standard Lagrangian hydro codes are incapable of modeling semi-collisional plasmas. The cells in Lagrangian meshes cannot interpenetrate leading to stagnation of the modeled collision which results in overestimates of density and temperature in the interaction region and rebounding shock waves. Modified Lagrangian techniques use two meshes which may overlap. The interaction of the two meshes is

controlled by terms which use parameters from the overlaying cells to calculate the coupling[3]. Other modified multi-fluid Lagrangian techniques have a third overlaying mesh describing the neutralizing electrons for example in an Eulerian mesh which regulates the interaction of the two colliding ion meshes[9]. More recently, particle-in-cell (PIC) techniques have been applied. In particular, the code ISIS[10] has been compared with other codes[11] in modeling the experiments described here. ISIS is an electromagnetic particle code which treats ions of each species separately in a kinetic fashion and the electrons as a massless fluid; explicit ion-ion as well as electron-ion collision effects are included. The interaction is modeled via a "collisonal field" that locally conserves both momentum and energy.

In this paper, we will describe colliding plasma experiments similar to those of Ref. 4. The experiments described here concentrated on high-Z and plastic coated high-Z target colliding plasmas because of initial interest with respect to ICF experiments using Au and CH coated Au hohlraums. We have also done preliminary spectroscopy experiments using Ti-Cr alloy targets. The range of Z-values and resulting plasma temperatures results in collisions which span the regimes from highly collisional in the high-Z case to interpenetrating in the case of the plastic plasmas. The experiments have generated data for comparison with codes such as ISIS.

ANALYTICAL CONSIDERATIONS

Simple arguments have been put forth which indicate which plasma parameters are most influential in controlling the degree of collisionality[3,11]. The plasma formed by irradiating a foil with a fast-pulse laser will expand somewhat isothermally. The fast particles in the ion velocity distribution will expand with velocities v_i several times the plasma sound speed given by

$$v_i = MC_S \tag{1}$$

where the M is the Mach number with a likely value of $1 \le M \le 3$ and the sound speed, C_s, is given by

$$C_S = \sqrt{\gamma Z k T_e / m_i}\ . \tag{2}$$

In Equation 2, Z is the ion charge, T_e is the electron temperature, m_i is the ion mass and γ is the ratio of specific heats of order 1. During expansion the effective ion temperature drops as the thermal energy is converted to kinetic energy. The electrons are carried along and the electron temperature decreases only slightly. The kinetic energy of the expanding fast ions given by

$$E_i = \frac{1}{2} m_i v_i^2 = \frac{1}{2} M^2 \gamma Z k T_e \tag{3}$$

can be $\gtrsim$100 keV for typical laser-target interaction conditions. Allowing two similar expanding laser plasmas to collide, using Eq. 1, the collisional mean free path λ can be approximated by[12]

$$\lambda \cong 3 \times 10^{13} \bullet \frac{M^4}{n_i \ln \Lambda} \left(\frac{\gamma T_e}{Z} \right)^2 \tag{4}$$

where $\ln\Lambda$ is 5 to 10 for typical values of the plasma parameter Λ. Eq. 4 indicates that the collision strength is highly dependent on T_e and Z and only weakly dependent on the ion density n_i. For Au targets irradiated with $\sim 10^{15}$ W/cm^2 of laser light, T_e = 2 keV and Z = 50 are typical. Taking M = 3, γ = 5/3, n_i = 10^{20} and $\ln\Lambda$ = 7, the high energy ion velocity given by Eq. 1 is 8.6 $\times$ 10^7 cm/sec. From Eq. 3, the high-energy ions would then have energies of 750 keV, and the collision mean free path from Eq. 4 is only 10 μm. However, because of the strong Z dependence in Eq. 4, for a low-Z element such as carbon

where $Z = 6$ and taking $\ln \Lambda = 10$, $\lambda = 480$ μm. Correspondingly for carbon, $v_t = 1.2 \times 10^8$ and $E_t = 90$ keV.

Eq. 4 indicates that by adjusting the values of Te and Z via either the target material or the laser power, the degree of stagnation of the plasma collisions can be controlled from a regime of abrupt stagnation to one of semi-collisional stagnation where the ion streams interpenetrate. The high kinetic energies in the ion streams indicated by Eq 3 are converted to thermal energy during the collisions resulting in x-ray emission which provides a useful means to diagnose the collision properties. X-ray emission from the initial laser-target interaction can be used to diagnose the plasma conditions before collision.

EXPERIMENT DESCRIPTION

Two types of laser targets geometries were used; the more complicated of which, called a "tuna

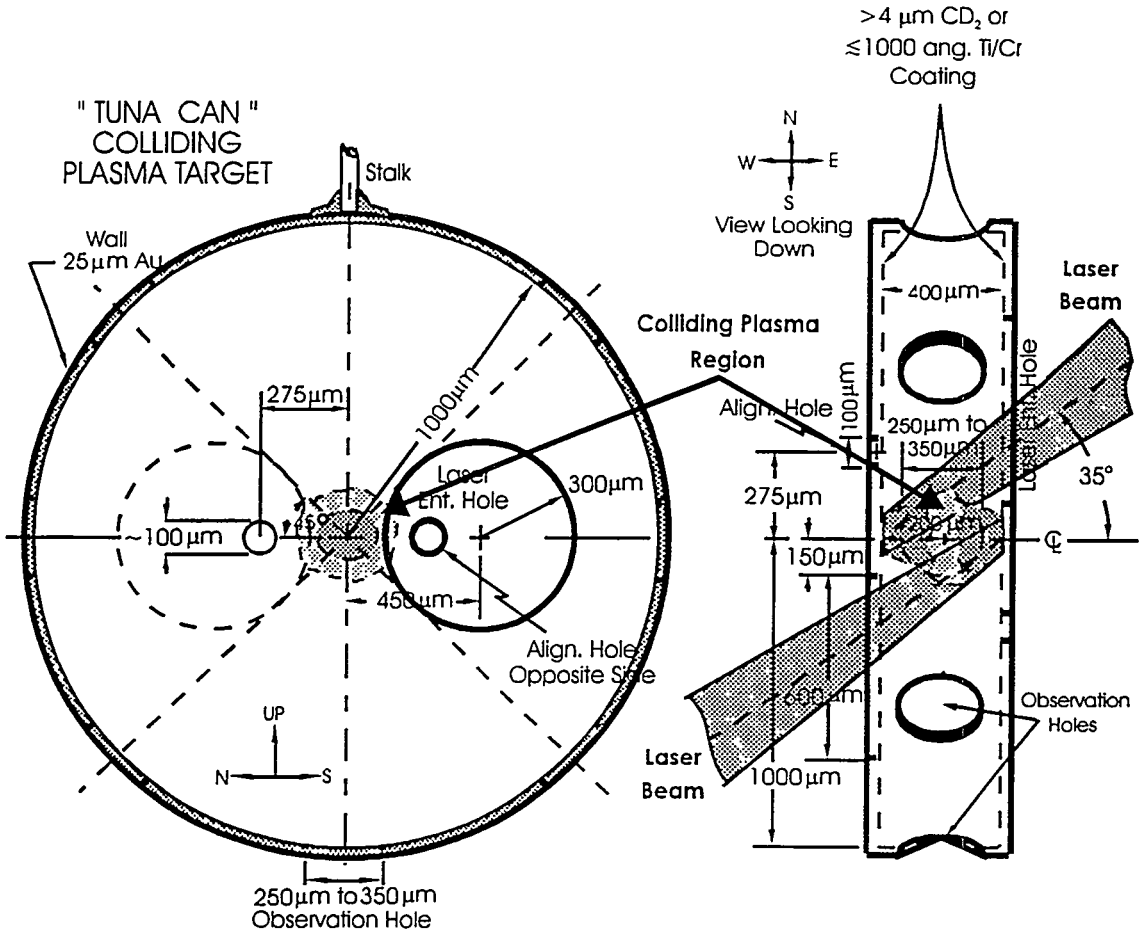

Figure 1. Schematic of laser targets showing illumination scheme and colliding plasma region.

can" is schematically represented in Fig. 1. The targets were formed from 25 μm thick Au. Plastic targets were formed by coating the inner surfaces with ≥ 4 μm of CD. Calculations indicated that for times of interest, layers of CD thicker than 2 μm did not burn through and were effectively infinitely thick. Several experiments were tried where the Au surfaces were coated with an 850 Å, 50%-50% alloy of Ti and Cr to obtain isoelectronic spectra for determination of temperature.

Two laser entrance holes allowed illumination of the opposing plates which were 400 μm apart at an angle of 35 degrees from the surface normal. The laser beams were focused to 120 μm diameter spots. Because of the angle, the illuminated region was an ellipse 120 μm in the vertical by 150 μm in the horizontal. The beams typically had 100 J of 2ω Nd-glass, 527 nm laser light each. The majority of data were taken with a 500 ps FWHM trapezoidal laser pulse with an 80 ps rise and 100 ps fall time.

The outer ring of the cylinder in Fig. 1 contained observation holes spaced every 45 degrees from the vertical. The holes acted as collimators so that the diagnostics only observed the collision region. The holes vinnetted emission from the laser target interaction region. Hole diameters were varied from 250 μm to 350 μm depending on the diagnostic requirements. When it was desirable to measure the emission from the target surface, a simpler "dual disk" target without the collimator ring was used. The spacing of the two disks was maintained by a 400 μm square target stalk to which the disks were glued.

X-ray instrumentation consisted of a 100 ps gated x-ray pinhole imager (GXI)[13], a time-integrated bremsstrahlung x-ray spectrograph and a gated imaging spectrometer (GIS) x-ray spectrograph used to record isoelectronic spectra from the Ti-Cr plasmas. In addition, the diagnostics included an ion spectrometer[14] and neutron detectors to measure D-D neutrons.

The GXI consisted of an array of 16, 10 μm pinholes in four rows of four each which produced 16 images; four images on each of four Au-strip cathodes. The magnification was 4 so that the images had about 40 μm resolution at the target. The Au strips are sequentially gated with variable delay. The gate pulses propagate down the Au strips gating each of the 4 images on a strip sequentially with 60 ps separation and about 100 ps gate width. The CD plasma images were filtered with a total of 13 μm of Be which cuts off below 1 keV x-rays. The images of the other plasmas were filtered with 140 μm of Be which produced a 2 keV cutoff.

The gated imaging spectrometer (GIS) was used to record the spectra of the He- and H-like spectra of the Ti and Cr coated targets. The GIS was a modification of the GXI where the front-end pinhole array was replaced with slits and a flat crystal. The four slits were aligned in the direction of the Au cathode strips. A PET crystal dispersed the x-rays along the Au strips to produce four spectra along each of the Au strips with spatial resolution across the width of each of the strips. Spectral coverage extended from 4.6 keV to 6.4 keV. The theoretical resolving power ($E/\Delta E$) was 6900. The $E/\Delta E$ of line widths measured here was always $\leq$1100.

A second, De Broglie-geometry time-integrated spectrometer was used to record the bremsstrahlung portion of the x-ray spectrum from a 500 μm field of view. The spectrometer had two channels. A PET channel covered 4.4 keV to 15 keV and a LiF channel covered 10.4 keV to 39 keV. The two time integrated spectra were recorded on an Au cathode micro channel plated detector coupled to a CCD camera. The spectrometer was absolutely calibrated at the BNLS synchrotron.

The ion detector was mounted along one of the 45 degree tangential lines of sight so that it received scattered ions from the collision. We attempted to measure direct ions normal to the surface of a single foil, but the sensitivity of the ion spectrometer and ion flux were such that it saturated. Also, the direct ion beams were intense enough that space charge inside the spectrometer disrupted the beams, confusing the traces of constant Z/m_i.

A rhodium counter activation detector[15] which had been previously calibrated[16] and a more sensitive calibrated 10 cm thick by 15 cm diameter fast plastic scintillator coupled to a 13 cm diameter photomultiplier tube were used to measure the total D-D neutron yield from CD colliding plasmas. The two detectors agreed within error limits. Attempts were made to make time resolved time of flight neutron measurements to determine the neutron energy distribution but the statistics were too low to make reliable measurements.

On occasion, a third 2ω, 500 psec beam of $\leq$20 J and variable delay was used to tangentially probe the plasma collision region. An optics system collect the stimulated Brillouin backscattered light and analyze the light on a streak camera coupled spectrometer[17].

IMAGING RESULTS

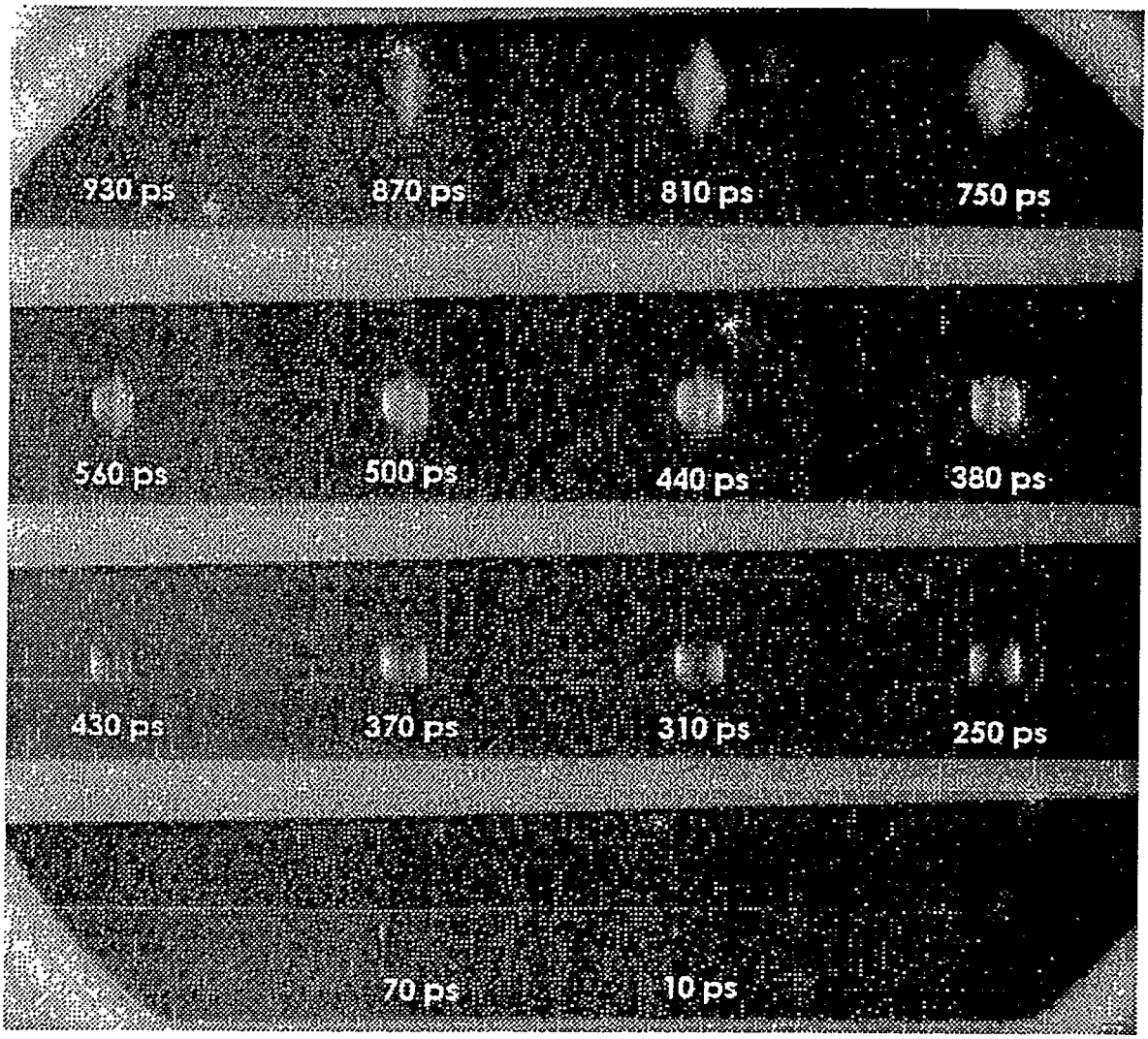

Fig. 2. GXI image of a Au plasma collision generated with a dual disk target.

A GXI image of a Au-target generated plasma collision is given in Fig. 2. In this case, a dual disk target was used so that the laser target interaction could also be imaged. The annotations indicate the time relative to the laser pulse breakout in picoseconds. Relative timing errors between images on different strips are accurate to 30 psec. Absolute timing to the laser pulse is accurate to 80 psec. The image has been corrected for the non-linear film response and we have also applied flat-field uniformity corrections. The spatial scale is measured at the GXI photocathode and must be reduced by the magnification factor of four to translate the scale to the target.

It can be seen that a stagnation has developed by 370 ps. If we take the time of stagnation as 350 ps and a distance of 200 μm. the velocity is 5.7×10^7 cm/sec, and from Eqs. 1-3, $M = 2$ and $E_i = 330$ keV. Eq. 4 would then imply that the collision mean free path, λ is 2 μm. Profiles of the images indicate that the collision region is 40 μm which is the pinhole resolution limit. Data from the ion spectrometer indicated that Au ions were scattered into the spectrometer with values of Z between 30 and 50 and with $E_i = 350$ keV. Similar evidence of high energy carbon (10 to 20 keV) and deuterium (2 to 7 keV) was obtained.

Neutron yields confirm the existence of the high energy deuterium ions. Although there was approximately 50% variation. yields for dual disk and CD coated tuna cans were 2 to 5×10^6 neutrons consistent with the ion energies measured with the ion spectrometer. Yields from targets where only a single laser beam was used gave yields that were a tenth to a half of dual beam shots.

Figure 3 shows an expanded view of the 560 ps image from Fig. 2. Also shown are images at 510 ps of Ti/Cr alloy-coated and CD-coated target plasma collisions. Figure 4 is a set of horizontal profiles from the images of Fig. 3. The measured horizontal profiles are an average of the central 100 μm (referenced at the target) of the image. The Au collision is distinct. Note that there is little emission from the disk on the right side of the image because of the 2 mm target disk diameter and the effects of parallax on images from the off-center pinholes. The Ti/Cr collision shows material emitting in the region between the disks although the collision scale length is on the scale of the disk separation. The CD collision shows almost no stagnation and the ions appear to freely interpenetrate.

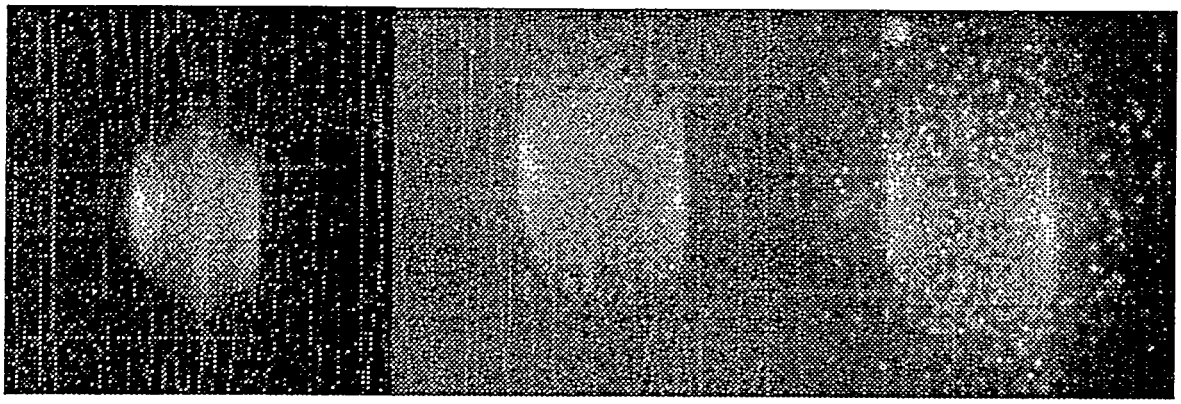

Fig. 3. An expanded view of the 500 ps image from Fig. 2. (left), and GXI images at 510 ps of Ti/Cr alloy-coated (center) and CD-coated dual disk target (right) plasma collisions.

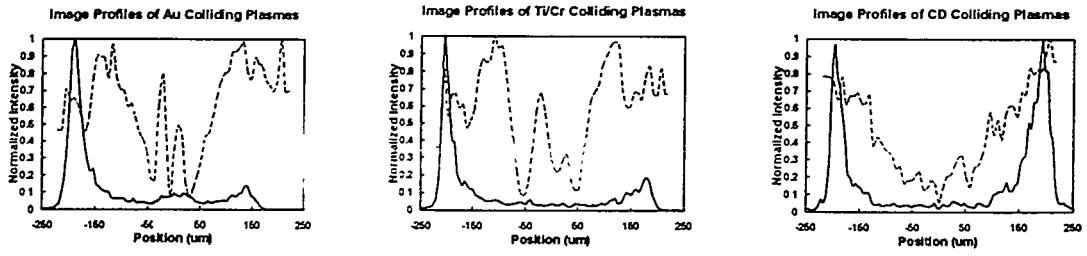

Fig. 4. Normalized horizontal profiles from the images of Fig. 3 plotted as solid lines and corresponding ISIS calculations plotted as dashed lines.

Also shown in Fig. 4 are ISIS PIC modeling calculations of the images of the collisions in Fig. 3. ISIS predicts collision scales consistent with the images. Details of the calculation can be found in Ref. 11. The calculations were initiated assuming a 25 μm slab of plasma at the target surface. The initial plasma ionization state and other plasma properties are based on the results of laser-target interaction calculations. Lagrangian calculation using Lasnex[18] predicted an initial Au electron temperature of 4 keV and an ionization state of 50. For the ISIS calculations to obtain the correct stagnation lengths and timing, an initial value of T_e = 2 keV was required. As expected Lasnex predicts that all cases will show an $\simeq$100 μm stagnation region between the disks, while the ISIS correctly predicts the interpenetration of the CD coated targets. It appears that ISIS also predicts stagnation of the Ti/Cr plasma. Close examination of the GXI images shows a faintly enhanced emission in the collision region however, not to the extent that ISIS predicts.

TEMPERATURE MEASUREMENTS

Because of the difference in T_e between the value required by ISIS to get the correct stagnation lengths vs. Lasnex laser target interaction calculations, and because of the strong dependence on T_e given in Eq. 4, several methods were used to measure the value.

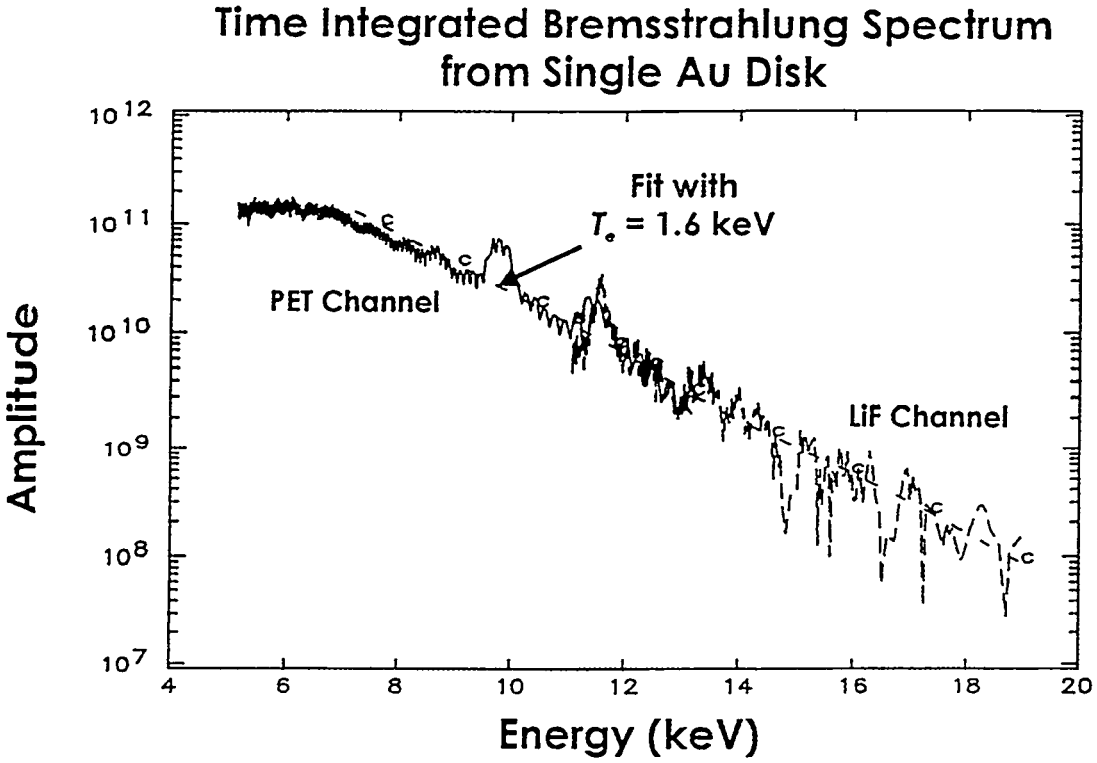

Fig. 5. Bremsstrahlung spectra from a single Au disk target and best fit to data indicating a T_e = 1.6 keV.

Results from the high energy spectrograph described above of a single Au disk with the spectrometer line of sight parallel to the target surface are given in Fig. 5. The spectra have been corrected for the spectrometer response, and the two spectra from the LiF and PET channels are spliced together. Also shown is a fit to the spectra assuming a exp($-h\nu/kT_e$) dependence. The best fit to the spectra which assumes a value of T_e = 1.6 keV is also plotted. Similar results were obtained for Au dual disk targets. The best fit value of T_e for Au tuna can targets was slightly higher; T_e = 2.0 keV, indicating that the majority of the plasma temperature in the collision region was still low. The derived values of T_e were

highly repeatable. For Ti/Cr and CD, the corresponding values of T_e are 1.2 ± 0.2 keV and 1.4 ±0.2 keV respectively. Results from the SBS backscatter measurements gave spectral shifts for Au targets which were also low; 1.3 keV for Au dual disks and tuna can targets.

The third type of temperature measurement using isoelectronic spectra has been attempted, but only preliminary results have so far been obtained. We attempted to deposit a non-perturbing layer of Ti and Cr alloy. In order to guarantee a known ratio of Ti to Cr, so far as mentioned above, the layers have been 850 Å thick. Experience should allow us to deposit thinner layers in the future. As ISIS calculations have shown, even 200 Å perturbs the Au stagnation. The 850 Å is essentially infinitely thick and there is little effect from the Au. This has been verified by the fact that the spectra show only the faint traces of Au M-lines. The use of spatially resolving slits in our initial attempts has yielded only faint spectra in the collision region. So far we have only analyzed spectra with large slits and hence spatially integrated. Because the current GIS line of sight is offset about 15 degrees in the equatorial plane, the use of the tuna cans to define the line of sight requires a repositioning of the apertures to avoid totally obscuring the plasma region. Therefore our initial spectral measurements have concentrated on Ti/Cr coated dual disks.

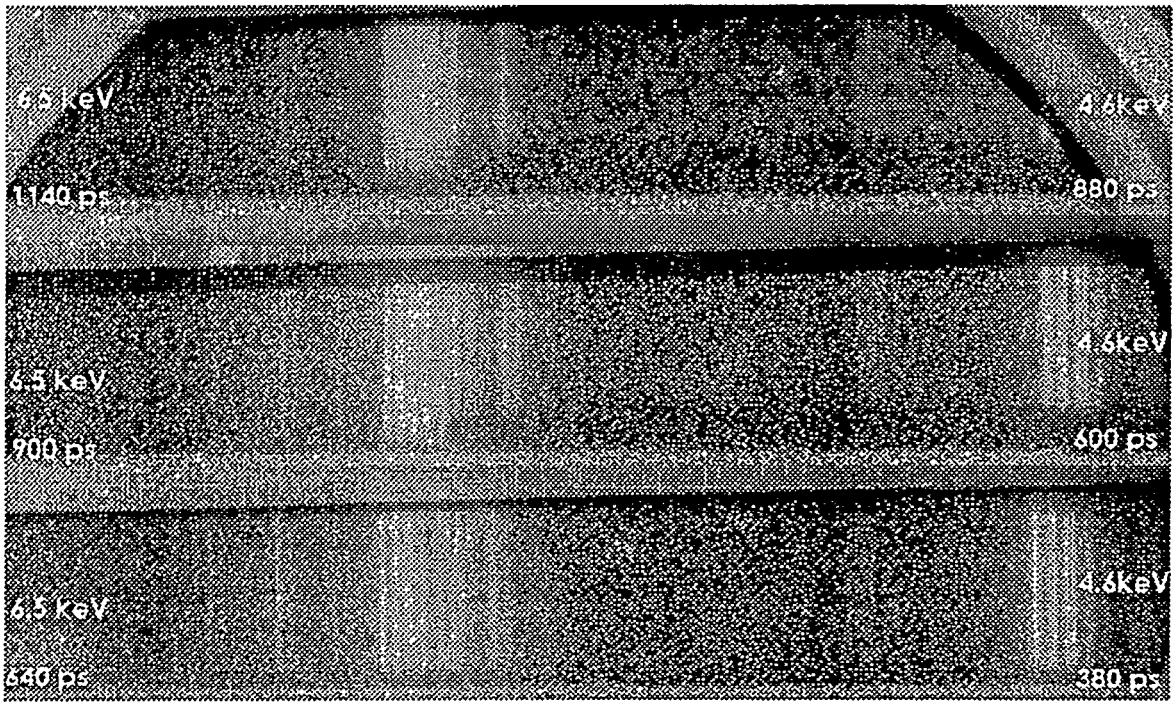

Fig. 6. GIS image of Ti/Cr spectra from a dual disk target generated plasma. The exposure times are indicated along with the approximate energy range of each spectra.

We have obtained spatially integrated spectra of the dual-disk Ti/Cr plasmas as shown in Fig. 6. The GIS snapshot times are given in the figure. Note that there is a delay from one side of the image to the other due to the finite propagation time of the gating pulse across the image. Only three of the four images from the shot in Fig 6. yielded good spectra. The energy scale increases from ~4.6 keV at the right to 6.4 keV at the left of the image. The profile generated by vertically averaging the central 25% of the spectra from the lower image (380 ps to 640 ps) is given in Fig. 7. Here we have plotted the energy scale from left to right and corrected for relative response across the image and corrected for response variation of the spectrometer versus energy.

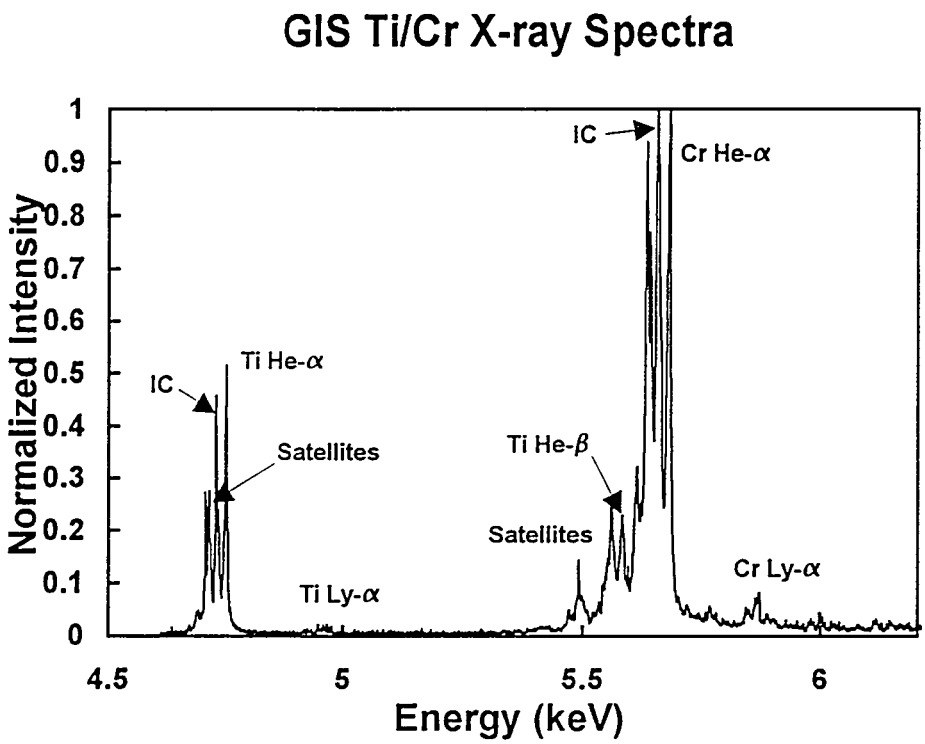

Fig. 7. Spectra from the lower image in Fig. 6 showing the He- and H-like lines of Ti and Cr.

The H- and He-like lines of Ti and Cr are evident in the spectra. Preliminary modeling of the spectra has been done using detailed fine structure atomic models for the Be-like through H-like ion stages of both titanium and chromium using the Los Alamos suite of atomic physics codes[19,20]. The calculations included the effects of intermediate coupling and configuration interaction. The level structure corresponding to the major configurations were calculated for the Be-like, Li-like, He-like and H-like ion stages.

Oscillator strengths were calculated for all dipole allowed transitions. Plane-Wave-Born collision strengths for electron impact excitation were calculated for all possible transitions. The distorted wave approximation (DWA) was used to calculate collision strengths for the most important transitions. Thus, the current model includes complete collision mixing levels. Detailed level-to-level collisional ionization cross sections, photoionization cross sections, and autoionization rates were also calculated. The calculated atomic physics data are based consistently on the same set of atomic wave functions and energy levels.

The effects of collisional excitation, collisional de-excitation, spontaneous radiative decay, collisional ionization, three-body recombination, radiative recombination, autoionization, and dielectronic recombination were included in the rate equations. The important mechanisms for populating the autoionizing levels are direct collisional excitation and dielectronic capture. The level populations were obtained from the steady-state or large time solution of the time-dependent rate equations. For this case, the problem reduces to the solution of a set of linear equations which depend on the electron temperature T_e and the electron density n_e. The intensities of spectral lines were predicted using the calculated populations and spontaneous emission rates described above. Line ratios were obtained by dividing the

appropriate line intensities. Isoelectronic line ratios are obtained by considering the same transition for two different elements with similar atomic numbers.

The steady-state population distributions were calculated for values of T_e between 1 and 10 keV, and n_e between 10^{19} and 10^{23} for both titanium and chromium. The atomic modeling indicated it was necessary to include optical depth effects to simulate the observed spectrum. Escape factors were used to account for these effects. Calculated line ratios were then generated as well as model spectra to compare with the data. The ratio for the Cr He-like resonance 2-1 line to the Ti He-like resonance line was observed to have a value of approximately 2. This value corresponds to temperatures above 5 keV for the range of densities studied. The best fit to the data were obtained at n_e near 10^{23} and for plasma sizes of a few hundred microns. The required density and plasma size to match the observed spectra is consistent with emission near the target surfaces. The large temperature however is inconsistent with the lower Te required in ISIS calculations to match the observed stagnation lengths.

Temperatures obtained from other line ratios assuming the plasma are also higher (4 to 6 keV) than the temperatures of $T_e \lesssim 2$ keV determined from backscatter or the bremsstrahlung spectra. We have not yet been able to reconcile this difference. So far, plasma conditions from the various plasma modeling codes have not been used to determine the plasma optical thickness although we plan to do this. The finite propagation of the gate pulse across the image may weight the later Cr lines. It is also possible that the Ti/Cr spectra is dominated by emission from a hot localized area whereas the bremsstrahlung spectra are more indicative of the bulk plasma temperature.

Line widths in the spectrum of Fig. 7 are $\simeq$6 eV, which is greater than the instrument resolution, and consistent with ion temperatures $\gtrsim$4 keV. The faint, spatially resolved spectra we have so far obtained indicate in the region of collision, that the lines appear to be several times broader possibly due to broadening from the collision and heating of the high-energy ions during emission. Analysis is underway.

CONCLUSIONS

The experiments described here are able to produce colliding plasmas with varying degrees of stagnation and interpenetration as evidenced by x-ray imaging. The variation of collisionality from stagnation to interpenetration provides useful data for comparison with modeling codes. Modeling comparisons were demonstrated by the agreement between the PIC code ISIS and both the CD and Au plasmas as opposed to a Lagrangian code, Lasnex, which is incapable of predicting the interpenetration in the case of the CD plasmas. The degree of collisionality depends strongly on the Z and T_e of the colliding species and to a lesser extent on the density. High-energy ions have been observed from the targets as predicted from simplistic arguments and modeling with ISIS which have energies consistent with the stagnation lengths and times. Determination of T_e from x-ray spectroscopic measurements of the bremsstrahlung and from backscatter measurements indicate an initial value of T_e consistent with that required to obtain the correct stagnation lengths for modeling of the plasma with ISIS.

So far we have been unable to reconcile the high-temperatures indicated from isoelectronic x-ray spectral measurements from Ti/Cr coated targets. We plan to continue these measurements with several refinements which should improve spatial resolution and our understanding of the source of the discrepancy.

ACKNOWLEDGMENTS

This work was performed under the auspices of the US Department of Energy. The authors thank R. Johnson, J. Goddard, N. Okamoto, S. Reading and F. Archuleta for operating the Trident laser during these experiments. We thank K. Alrick, J. Faulkner, T. Hurry, R. Carrow, G. Schmidt and S. B. Boggs for their technical assistance in the areas of setup and data recording. We also thank P. Gobby and H. Bush for providing the targets used for these experiments, R. Hockaday for technical advice concerning the GIS

spectrometer, M. M. Shauer and K. Klare for technical assistance concerning the data reduction and R. Chrien for advice regarding the use of the neutron activation detector.

REFERENCES

1. N. A. Krall and A. W. Trivelpiece, *Principles of Plasma Physics*, McGraw-Hill Book Company, New York, 1973.
2. Ya. B. Zeldovich and Yu. P. Raizer, *Physics of Shock Waves and High-Temperature Hydrodynamic Phenomena*, Ed. W. D. Hayes and R. F. Probstein, Vols. I and II, Academic Press, New York, 1966-67.
3. R. Berger, J. R. Albritton, C. J. Randall, E. A. Williams, W. L. Kruer, A. B. Langdon and C. J. Hanna, "Stopping and thermalization of interpenetrating plasma streams," *Phys. Fluids B* **3**, pp. 3-12, Jan. 1991.
4. R. A. Bosch, R. L. Berger, B. H. Failor, N. D. Delameter, G. Charatis, and R. L. Kauffman, "Collision and interpenetration of plamas created by laser-illuminated disks," *Phys. Fluids B* **4**, pp. 979-988, Apr. 1992.
5. S. M. Pollaine, R. L. Berger and C. J. Keane, "Stagnation and interpenetration of laser-created colliding plasmas," ," *Phys. Fluids B* **4**, pp. 989-991, Apr. 1992.
6. P. Glas, M. Schnürer, E. Förster and I. Uschmann, "X-ray microscopy of laser produced counterstreaming plasmas-investigation of population inversion in [He]-like Al," *Optics Com.* **86**, pp. 271-276, 1991.
7. C. Stöckl and G. D. Tsakiris, *Laser Part. Beams* **9**, pp. 725-747, 1991.
8. O. L. Landen, Lawrence Livermore Lab., Private communication.
9. S. A. Bel'kov, P. D. Gasparyan, G. V. Dolgoleva, N. V. Zhidkov, N. V. Ivanov, Yu. K. Kochubej, G. F. Nasyrov, V. A. Pavlovskii, V. V. Smirnov, V. G. Rogatchev, and Yu. A. Romanov, VNIIEF unpublished report (part 3), 1993.
10. M. E. Jones, V. A. Thomas, and D. Winske, "An Interparticle Collision Model for Electromagnetic Hybrid Simulations of High Density Plasmas," *Proceedings of the 14th Conf. on Num. Sim. of Plasmas*, Annapolis, MD, 1991.
11. M. E. Jones, D. Winske, S. R. Goldman, R. A. Kopp, V. G. Rogatchev, S. A. Bel'kov, P. D. Gasparyan, G. V. Dolgoleva, N. V. Zhidkov, N. V. Ivanov, Yu. K. Kochubej, G. F. Nasyrov, V. A. Pavlovskii, V. V. Smirnov and Yu. A. Romanov, "Ion Interpenetration, Stagnation and Thermalization in Colliding Plasmas: 1. Numerical Modeling", Los Alamos Report LA-UR 95-1625, submitted to *Phys. Plasmas*, 1995.
12. L. Spitzer Jr., *Physics of Fully Ionized Gases*, Wiley (Interscience), New York, 1962.
13. J. A. Oertel, T. Archuleta, S. Evans, J. Jimerson, T. Sedillo and R. G. Watt, "Gated X-ray Images of Nova Hohlraums," Los Alamos Report DRR-94-10-LA, June 1, 1994.
14. G. Guethlein, J. Bonlie, D. Price, R. Shepherd, B. young and R. Stewart, "Charge and mass resolved time of flight observations of 140 fs laser produced ions," *Rev. Sci. Instrum.*, **66**, pp. 333-335, January 1995.
15. C. A. Ekdahl, "Neutron diagnostics for pulsed high-density thermonuclear plasmas," *Rev. Sci. Instrum.*, **50**, pp. 941-948, August 1979.
16. R. E. Chrien, "Neutron calibration for the FRX-C/LSM magnetic compression experiment," *Rev. Sci. Instrum.*, **62**, pp. 1489-1493, June 1991.
17. B. S. Bauer, R. P. Drake, K. G. Estabrook, J. F. Camacho, R. G. Watt, M. D. Wilke, G. E. Busch, S. E. Caldwell and S. A. Baker, "Meeting the challenge of detecting ion plasma waves," *Phys. Plasmas*, **2**, pp. 2207-2215, June 1995.
18. G. B. Zimmerman and W. L. Kruer, "Numerical Simulation of Laser-Initiated Fusion," *Comments Plas. Phys.*, **2**, pp. 51-61, 1975.
19. J. Abdallah, Jr. and R.E.H. Clark, "Theroetical Atomic Physics Code Developement," Los Alamos National Laboratory reports, LA-11436-M, I-V, 1988.
20. J. Abdallah, Jr., R.E.H. Clark, C. J. Keane, T. D. Shepard and L. J. Suter, "Radiation Field Effects on the Spectroscopic Properties of Seeded Plasmas," *J. Quant. Spectrosc. Radiat. Transfer*, **50**, pp. 91-101, January 1993.